IEEE Access
Multidisciplinary | Rapid Review | Open Access Journal

Received 24 September 2023, accepted 3 October 2023, date of publication 9 October 2023, date of current version 13 October 2023.

Digital Object Identifier 10.1109/ACCESS.2023.3322923

RESEARCH ARTICLE

Design of 150°C DC–DC Converter Based on Flyback Topology for Downhole Drilling Equipment

FEI LI, YUAN LIU, XUEYING MA, AND YUQI TAN
School of Electrical Engineering, Xi'an Shiyou University, Xi'an 710065, China

Corresponding author: Fei Li (lif@xsyu.edu.cn)

This work was supported in part by the National Science Foundation of China under Grant U20B2029, in part by the Natural Science Research Program of the Department of Science and Technology of Shaanxi Provincial under Grant 2022KW-25, and in part by the Xi'an Shiyou University Postgraduate Training Program for Innovation and Practice Ability under Grant YCS22214234.

ABSTRACT High temperatures in unconventional oil and gas reservoir present a challenge to DC-DC converter design for downhole drilling equipment. In response to the high-temperature challenge, a design methodology consisting of controlling-junction temperature rise, derating component electrical parameters for more design margin and selecting high-temperature components was proposed. Based on the methodology, a converter board with a nominal input of 42-54V and output of three low voltages (+15V, −15V, and +5V), was designed for the 150°C application. The maximum temperature rise of the components in the converter prototype under a temperature environment of 22°C is 11.9°C. The performance of the converter was verified at the ambient temperature from 30°C to 150°C. With a 42∼54V input voltage, the output voltages have less than 0.2V fluctuation; the three output voltages can achieve a ripple suppression ratio of approximately 40dB, and the average conversion efficiency was around 75% at 150°C, which meets the design specification.

INDEX TERMS DC–DC converter, high-temperature design, flyback topology, derating design.

I. INTRODUCTION

The exploration and development of unconventional oil and gas reservoirs have developed rapidly globally [1]. Unconventional oil and gas have become an essential part of the oil and gas supply system [2]. As a crucial technology for the development of unconventional oil and gas fields, rotary steerable system (RSS) has attracted growing attention and research efforts from scientific institutions and oilfield service companies [3]. The most widely used power supply system in the RSS is the turbine mud generator system. After the AC power output of the generator is converted into electric energy of AC-DC through rectification technology, the DC-DC converter is needed to provide electric energy to the electronic warehouse and other electronic devices in the downhole of the system [4], [5]. The operating temperature of RSS is usually between 150°C and 170°C, with a geothermal temperature gradient of 3°C/100m. For oil and gas wells with depths ranging from 6,000 to 7,000 meters, the highest temperature at the bottom of the well is approximately 180°C-210°C or even higher [6], [7], [8]. In the work of the underground power supply, it is difficult for the circuit board to exchange heat with the surrounding environment, so the designed high-temperature converter circuit is required to overcome the challenges brought by the underground high-temperature environment [9], [10], [11].

According to the statistics of electronic equipment failure caused by environmental factors from national aeronautics and space administration (NASA), the failure rate of electronic systems caused by ecological temperature is as high as 55% [12]. In the downhole high-temperature environment, the semiconductor components of the average temperature converter and their circuits are challenging to work reliably [13], [14]. High temperatures lead to changes in the

The associate editor coordinating the review of this manuscript and approving it for publication was Jiann-Jong Chen.

TABLE 1. Converter design specification.

Parameter	Value
Input voltage(V)	42~54
Output voltage V_{dc}(V)	Vo1: +15(5W) V_{O2}: -15(4W) Vo3: +5(3W)
Efficiency (%)	>75
Frequency (kHz)	95
Maximum operating Temperature (°C)	150

performance of electronic devices and even damage to the devices. Therefore, during the component selection process, it is imperative to consider the maximum operating temperature provided in the datasheet to ensure the optimal performance and normal operation of electronic devices [15]. The most important thing is the electrical parameter changes of semiconductor devices, among which the electrical performance specifications such as breakdown voltage, leakage current, amplification factor, and allowable power are positively or negatively correlated functions of temperature [16]. Other factors include decreased carrier mobility, increased electron migration in metal interconnects, and decreased dielectric breakdown strength [17], [18]. In addition to the high temperature brought by the downhole environment, integrated circuits, switching devices, and other components in the circuit also generate heat during operation, resulting in a further temperature rise. Under the combined effect of downhole environment temperature and temperature rise, the losses of electronic components in the circuit are further increased [19]. If the high temperature in the working environment of the converter is not considered during the initial design, the converter circuit in the equipment will suffer from reduced performance and shortened lifespan. In addition, the increase in temperature will lead to increased internal losses in the components, which may eventually result in circuit malfunction [20]. Therefore, studying the high-temperature design of DC-DC converter is significant.

This paper is organized as follows. The technical specifications and architecture of high temperature converter are presented in Section II. Section III presents the design methodology of high-temperature converter. The test environment built, and the normal temperature function and high temperature performance are verified presented in Section IV. The conclusion is given in Section V.

II. DESIGN SPECIFICATIONS AND STRUCTURE OF HIGH-TEMPERATURE CONVERTER

In the design of high-temperature power supplies, a thorough understanding of various converter performance specifications is required as a starting point to select a design solution that meets the design requirements. As shown in Table 1, multiple technical specifications are listed for the conditions of the design converter.

According to the design specifications, the converter needs to have the anti-interference ability, as well as the ability to isolate the electrical connection between the input and output terminals, presenting a high impedance state at both ends to block the current loop and prevent interference with the output of the subsequent converter. The converter demand of electronic instruments in RSS is diversified, requiring multi-terminal output capacity to avoid the complexity of converter system design, and the design specification requires a small power. According to the above statement, flyback topology is selected as the design basis of the system [21], [22], [23], [24]. According to the design requirements in Table 1, the schematic diagram of the designed flyback topology is shown in Fig. 1.

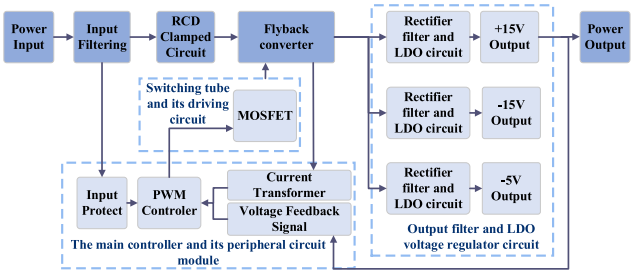

FIGURE 1. Block diagram of flyback converter.

This converter is designed in detail in six parts, including the input filter circuit module, the peak absorbing circuit (RCD) buffer circuit module, the flyback transformer module, the central controller and its peripheral circuit module, and the output filter and low dropout regulator (LDO) circuit module. The design of each circuit section was completed to realize the high-temperature converter prototype, which can meet the design requirements under both room temperature and high temperature.

III. HIGH-TEMPERATURE DESIGN METHOD OF CONVERTER

According to data from the U.S. Naval Electronic Laboratory, the probability of electronic equipment becoming unreliable due to circuit design is 40%, while device usage accounts for 30% of the causes [25]. Due to the complexity of the coexistence of drilling equipment and the downhole environment, it is difficult to carry out active and passive cooling measures. Theoretically, the operating temperature of the downhole high-temperature converter does not differ much from the temperature variation of the formation [26], [27], [28]. Therefore, to improve the temperature resistance of the overall circuit of the high-temperature converter, high-temperature reliability design should be considered from three aspects:

Such as the design of controlling temperature rise of components, derating use of electronic devices, and packaging of devices, as shown in Fig. 2.

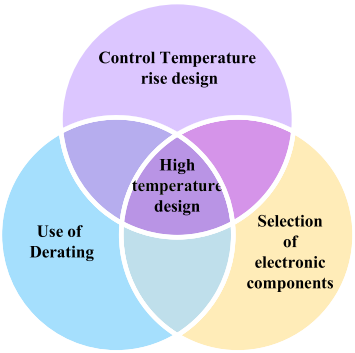

FIGURE 2. High-temperature circuit design factors.

A. TEMPERATURE RISE CONTROL

Due to the influence of parasitic parameters, semiconductor devices will result in some power loss, which causes the temperature of the device to be higher than the ambient temperature. As shown in Fig. 3, the TO-220 package of the switch MOSFET is taken as an example. T_A represents the ambient temperature, T_J represents the semiconductor junction temperature, and T_C represents the case temperature. There is thermal resistance between T_A and T_J thermal resistance T_C between T_J and R_{thJC}. Therefore, under different thermal resistance conditions, the device will experience a temperature rise higher than the ambient temperature, which can cause significant performance degradation and even damage the device when operating at or near the maximum operating temperature.

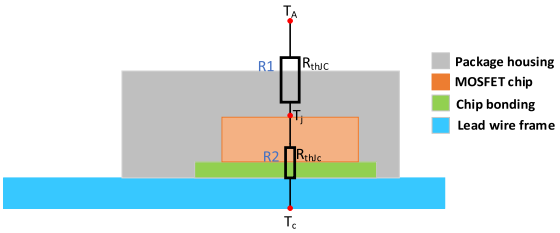

FIGURE 3. MOSFET thermal resistance model.

By employing techniques such as component layout, copper coverage, windowing, and heat dissipation holes on the PCB, rational and efficient channels with low thermal resistance can be established. Designing heat dissipation holes and blind holes around the heating element can effectively increase the heat dissipation area, reduce thermal resistance, and enhance the power density of the circuit board [29]. Significant heat-generating or high-current elements should be avoided from being placed at the corners and edges of the printed circuit board. A proper layout of circuit components and increased copper coverage can accelerate heat conduction. To enhance the heat dissipation capability of the TO-220 package, thermally conductive silicone grease is used to fill the gap between the heat sink of the MOSFET, the ceramic thermal pad and the metal lower frame to assist heat transfer. The installation is illustrated in Fig. 4.

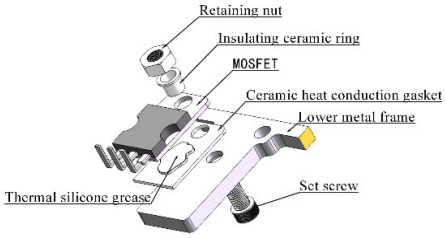

FIGURE 4. Schematic diagram of MOSFET installation.

To reduce the temperature rise and prevent deformation of the circuit board under high temperature, a metal upper and lower frame was used for reinforcement and auxiliary heat dissipation around the power devices. The structure of the metal frame is shown in the Fig. 5.

FIGURE 5. Design effect of high-temperature converter prototype.

In addition to protecting the device, different packaging forms correspond to power and application scenarios. Due to the limited ability of high-temperature power supplies to exchange heat with the environment, MOSFET packages with large heat sinks such as TO-220 are selected to dissipate the heat generated by the device to the entire circuit, reducing the temperature rise of the MOSFET and its surroundings. All power devices in the converter prototype are selected with TO-220 packaging, and the carrier of the devices is a printed circuit board (PCB) with a maximum operating temperature of 200°C. From the component selection and design perspective, this circuit can improve the overall temperature resistance performance [31], ensuring that semiconductor devices can generally operate under long-term high-temperature conditions.

B. THE DERATING USE OF HIGH-TEMPERATURE ELECTRONIC COMPONENTS

In high-temperature power supplies, the issue of component derating must be fully considered to reduce the probability of electronic component failure mechanisms. Therefore, the derating criteria were based on the "Technology specification for derating of electronic components of converter " [30], and the derating levels are shown in Table 2.

As the temperature of the device increases, the decrease in electrical performance parameters further increases power losses. Derating can effectively improve the reliability of electrical performance parameters of electronic components in extreme environments. However, derating usually increases the device's weight, size, and cost. Therefore,

TABLE 2. Technology specification for derating of electronic components of converter.

Derating grade	Application situation
Derate level 1(Maximum derating)	Non-recoverable damage occurs after an equipment failure, which requires high equipment reliability.
Derate level 2(Moderate derating)	Equipment failure may result in equipment damage and high maintenance costs.
Derate level 3(Minimum derating)	The consequences of equipment failure are slight, and the repair cost after loss is low.

derating needs to be considered in combination with all factors of electronic devices. Excessive derating may cause changes in the typical characteristics of the device or introduce new failure mechanisms. The converter design will reference the level-2 derating standard according to the derating level division. Choose to use reverse voltage, current, and power much higher than the calculated parameters to achieve the purpose of derating. In addition, most semiconductor device performance parameters increase is accompanied by a more significant on-state resistance, which requires careful consideration of the trade-off between derating and power loss.

C. SELECTION OF HIGH-TEMPERATURE ELECTRONIC COMPONENTS

In this converter, unconventional high-temperature components were selected for the six modules. By selecting high-temperature capacitors of different capacitance values, high-frequency interference, common-mode interference, and low-frequency interference of the input signal were effectively filtered out. The capacitors used were high-temperature tantalum capacitors (Exxelia). The switch IC used was SIC MOSFET (UnitedSIC), which can operate normally at 150°C.

At 150°C, high-temperature ceramic packaging is a reasonable solution, and therefore, majority devices used in this design are packaged in ceramics. The PWM controller used is UCC1806, which is a ceramic-packaged, low-power, dual-output current-mode PWM controller. The magnetic core of the transformer is made of Kool mu hf material, which has a Curie temperature of 500°C (Cruise temperature) and meets the design requirements at 150°C.

IV. TEST OF THE PROTOTYPE AT STANDARD TEMPERATURE AND HIGH TEMPERATURE

The temperature cycling test of the power prototype is used to simulate the high-temperature resistance of the downhole power prototype under the temperature cycle of 30-150°C during actual operation. Within the set temperature range, temperature rise, temperature maintenance, and temperature drop are counted as a cycle. Based on practical engineering experience, a testing cycle consisting of three temperature cycles was used. The temperature cycling test method for high-temperature converter refers to the process specified in GJB548B-2005 "Test Methods and Procedures for Microelectronic Devices" [32]. The test environment is set up as shown in Fig. 6(a) offers the external environment of the test, and (b) shows the internal environment of the high-temperature oven.

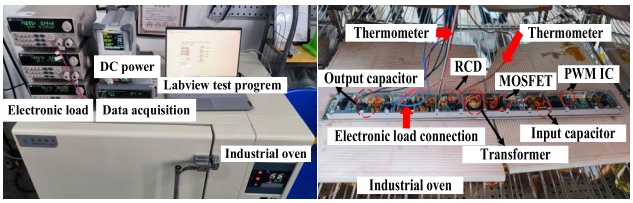

(a) (b)

FIGURE 6. (a)Test the external environment. (b) High-temperature oven internal environment.

Fig.7 (a) and (b) show the ripple comparison of the +15V line before and after filtering. The peak-to-peak value of the ripple before filtering is about 450mV. After filtering and linear regulation by the LDO circuit, the peak-to-peak value of the wave is about 4.2 mV. The ripple suppression effect is expressed by the ripple suppression ratio (*RSR*), as shown in the following equation.

$$RSR = 20 \log \frac{V_{IPP}}{V_{OPP}} \tag{1}$$

where V_{IPP} represents the peak-to-peak value of the ripple voltage of the input voltage, while V_{OPP} represents the peak-to-peak value of the ripple voltage of the output voltage. After calculation, the ripple suppression ratio of the +15V rail is 41dB.

Fig.7 (c) and (d) depict the ripple waveform comparison before and after filtering on the −15V path. The peak-to-peak ripple value before filtering is approximately 380 mV. After filtering and linear regulation through the LDO circuit, the peak-to-peak ripple value is about 3.0 mV, yielding a ripple suppression ratio of 42dB.

Fig. 7 (e) and (f) show the comparison of ripple waveform before and after filtering on the +5V path. The peak-to-peak ripple value before filtering is around 450mV. After filtering and linear regulation through the LDO circuit, the peak-to-peak ripple value is about 3.2mV, resulting in a ripple suppression ratio of 43dB.

Fig. 8 shows the testing of the heating conditions of the components on the experimental board under full load. The testing was conducted at an ambient temperature of approximately 22°C. After the temperature rise of the converter prototype stabilized, a thermal imaging technique was employed to measure the temperature rise of the clamp resistor of the RCD, the flyback transformer, the switching ic, and the output rectifier diode. Among them, the flyback transformer had the highest temperature rise, reaching 11.9°C, while the RCD had the lowest temperature rise, at 10.3°C.

Out of 100 cycles tested, three tests were selected as representative tests. The temperature cycles used in the test

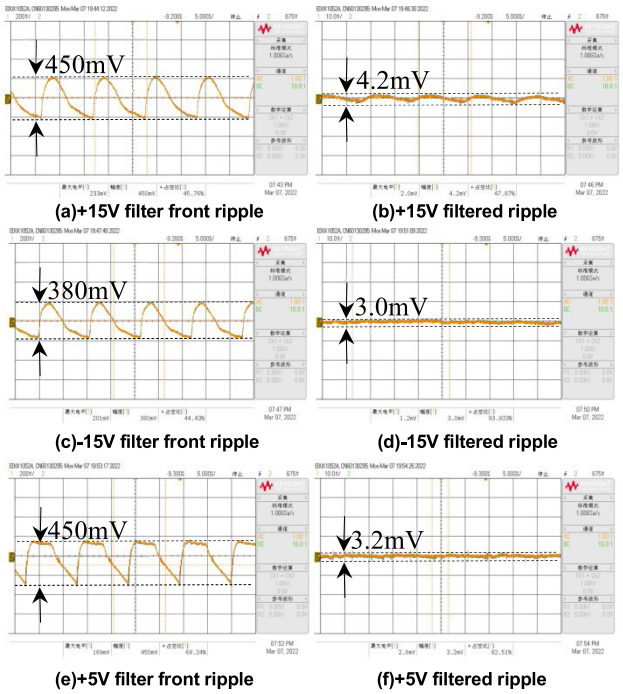

FIGURE 7. Critical circuit waveforms at normal temperature.

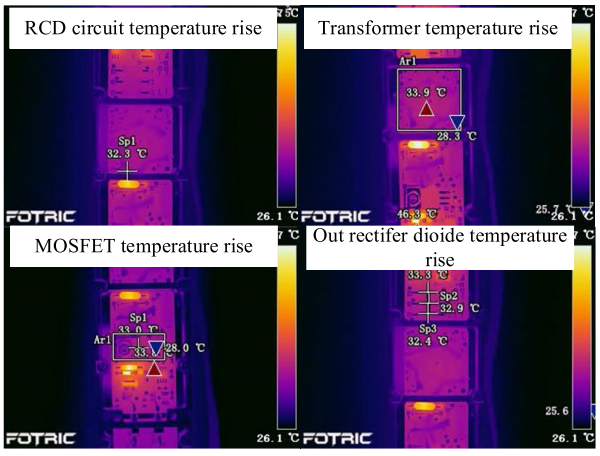

FIGURE 8. Maximum circuit temperature module at the average temperature.

are based on the previous underground environmental temperature survey. The environmental temperature rise in the high-temperature test should be controlled at 1-3°C/min, so the temperature change is set to 2°C/min during the three-cycle temperature rise process. The change of temperature rise in cooling is the same as the temperature rise process. During the test, the operating temperature of multiple devices was monitored, and the device temperatures at 22°C and 150°C inside the oven are shown in Table 3 below.

As can be seen from the above table, the working temperature of several critical components at 150°C is within the allowable range of the datasheet. The temperature rise

TABLE 3. Temperature rise of critical components undeer full load.

Main component	22°C	150°C	Datasheet/°C
PWM controller	22.5°C	150.5°C	125°C
Transformer	33.9°C	162.3°C	200°C
MOSFET	33.2°C	161.3°C	175°C
RCD	32.3°C	160.5°C	175°C
Input capacitor	22.89°C	150.89°C	200°C
Output capacitor	23.8°C	150.39°C	200°C
Metal frame	20°C	151.5°C	250°C

of the PWM controller exceeds the recommended operating temperature of the datasheet, but due to its ceramic package, it does not significantly exceed the maximum allowable operating temperature of 150 degrees Celsius stated in the datasheet. The military-grade device operated normally during the 100-cycle test. After the high temperature cycle, there is no obvious damage to the external components of the converter prototype, and the converter prototype can work normally. The full-cycle output data is collected during the high-temperature cycle test, and the output of the three channels is obtained after sorting.

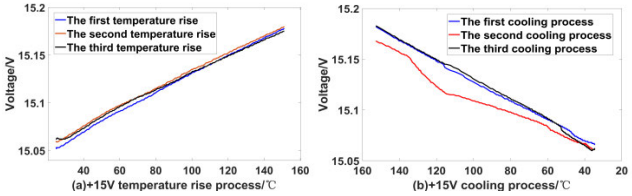

FIGURE 9. Output voltage variation of +15V in three cycles.

A. OUTPUT VOLTAGE VARIATION AT AN INTEGRAL PERIOD OF +15V

According to Fig. 9(a), it can be observed that during the three-cycle temperature rise of the +15V line, the temperature change range remains between 30°C and 150°C, and the voltage change remains between +15.05V and +15.20V, with a voltage change amplitude less than 0.2V. According to Fig. 9(b), during the three-cycle cooling process of the +15V line, the temperature range remained between 150°C and 30°C, and the voltage variation was maintained between +15.18V and +15.05V, with a voltage change amplitude less than 0.2V. The slope of the voltage change is consistent in the three cycles of temperature changes.

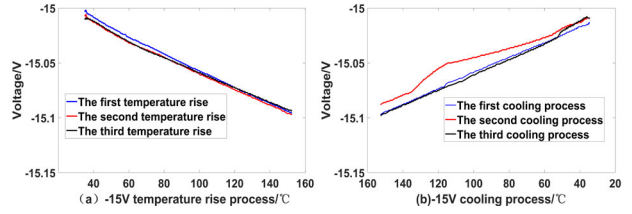

FIGURE 10. −15V Output voltage changes at three periods.

B. OUTPUT VOLTAGE VARIATION AT AN INTEGRAL PERIOD OF −15V

According to Fig.10(a), during the three-cycle temperature rise process of the −15V path, the temperature range remained between 30°C and 150°C, while the voltage variation remained between −15.03V and −15.11V. The output voltage exhibited oscillation between 90°C and 140°C, but the magnitude of the fluctuation was less than 0.2V. According to Fig. 10(b), it can be seen that during the three cycles of the cooling process of the −15V path, the temperature range remained between 150°C and 30°C, while the voltage range remained between −15.11V and −15.03V, with voltage variations all below 0.1V. The voltage changes slopes remained consistent throughout the three cycles of temperature change.

C. OUTPUT VOLTAGE VARIATION AT AN INTEGRAL PERIOD OF +5V

According to Fig.11(a), during the entire cycle, the temperature range of the +5V route in the temperature-rising process remained between 30°C and 150°C, while the voltage changes remained between +5.03V and +5.05V, with a voltage change amplitude of less than 0.1V. According to Fig. 11(b), during the cooling process of the entire cycle of the +5V path, the temperature range remained between 150°C and 30°C, and the voltage change remained between +5.03V and +5.05V, with voltage changes of all three cycles being less than 0.1V. The voltage change slope remained consistent in all three temperature cycles.

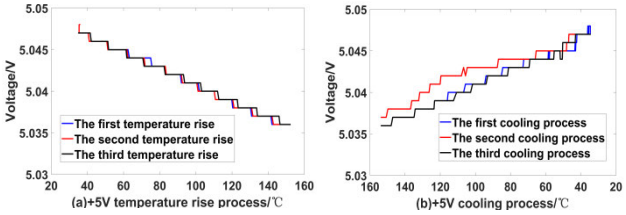

FIGURE 11. +5V three-cycle output voltage changes.

In the three-cycle temperature cycle, the efficiency formula of the high-temperature converter is:

$$\eta = \frac{V_{O1} \cdot I_{O1} + V_{O2} \cdot I_{O2} + V_{O3} \cdot I_{O3}}{V_{\text{in}} \cdot I_{\text{in}}} \times 100\% \quad (2)$$

where V_{O1}represents the output voltage1 (+15V), while I_{O1} represents the output current1; V_{O2}represents the output voltage2 (−15V), while I_{O2} represents the output current2; V_{O3}represents the output voltage3 (+5V), while I_{O3} represents the output current3; V_{in}represents the input voltage, while I_{in} represents the input current; η represents the efficiency of power prototype.

The test conditions are shown in Table 4:

The prototype was subjected to efficiency testing, and the overall efficiency of the converter was above 75% during the three-cycle high-temperature cycling test, meeting the design requirements. The results are shown in Fig.12.

TABLE 4. Efficiency test conditions of power prototype.

Test condition	Value
Input voltage	42-54V
Temperature test range	30°C-150°C
Output load (Full load)	+15V:49Ω -15V:59Ω +5V:9Ω

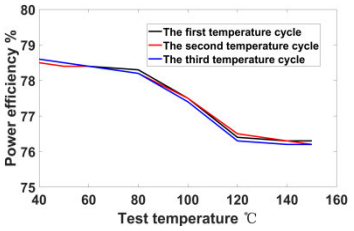

FIGURE 12. Efficiency change of power prototype under the three-cycle temperature cycle.

V. CONCLUSION

The design approach proposed in this paper, which combines temperature rise control, derating usage, and selection of electronic components, is applied to achieve the high-temperature performance of conventional power supplies. The feasibility of this method is verified by experiments. (1) By increasing the copper coverage and the number of through-holes on the circuit board, the heat dissipation area of the circuit board was increased. Using a metal frame further balanced the temperature rise of the circuit board, eliminating the impact of high temperature on electronic components caused by localized heat buildup. (2) Using reverse voltage, current, and power much higher than the calculated parameters to achieve the purpose of derating. (3) By selecting high-temperature components, the sensitivity of electronic devices to temperature variations was overcome, thereby enhancing the operational lifespan of the designed converter in a 150°C environment. In a three-cycle high-temperature test ranging from 30°C to 150°C, the variation range of the three output voltages is less than 0.2V. Additionally, the efficiency of the converter prototype remains above 75% throughout the three-cycle high-temperature test. The high-temperature testing demonstrated that the external integrity of the components remained intact with no visible damage. This satisfies the design requirements for the high-temperature DC-DC converter of the drilling measurement and control system for RSS. In future work, research will be conducted on the design methods of power circuits for even higher temperatures based on this foundation.

REFERENCES

[1] G. X. Li, Z. D. Lei, and W. H. Dong, "Challenges and prospects of unconventional oil and gas development of CNPC," *China Petroleum Explor.*, vol. 27, no. 1, p. 1, Jan. 2022.

[2] F. Z. Jiao, "Re-recognition of 'unconventional' in unconventional oil and gas," *Petroleum Explor. Developmen*, vol. 46, no. 5, pp. 803–810, Aug. 2019.

[3] D. Feng, P. Wang, and H. Zhang, "Research status and development trend of rotary steerable system tool," *China Petroleum Machinery*, vol. 49, no. 7, pp. 8–15, Jul. 2021.
[4] B. Bouldin, A. AlShmakhy, and A. K. Bazuhair, "A review of downhole wireless technologies and improvements," in *Proc. ADIP*, vol. 15, no. 11, Nov. 2021, pp. 15–18.
[5] Z. Da, B. Yuxin, and L. Xue, "Design of downhole mud turbine generator," *Petro Chem. Equip.*, vol. 26, no. 3, pp. 53–56, Mar. 2023.
[6] J. Gan, D. Wu, and Y. C. Zhang, "Distribution pattern of present-day formation temperature in the qiongdongnan basin," *Geolog. J. China Universities*, vol. 25, no. 6, 2019, pp. 952–960, Dec. 2019.
[7] Y. Jie, K. Ye, and W. Gao, "Design of half bridge SiC high temperature DC switiching power supply at 150?" *Adv. Technol. Electr. Eng. Energy*, vol 37, no. 10, pp. 71–76, Sep. 2018.
[8] W. Gao, K. Liu, Y. Su, L. Sheng, C. Cao, X. Dou, and L. Zhang, "Active cooling method for downhole systems in high temperature environment," in *Proc. Day 2 Wed, April 24*, Apr. 2019, pp. 23–26.
[9] P. K. Padhee and P. C. Sekhar, "Isolated multi-output power supply based on flyback converter," in *Proc. ICPEE*, vol. 71, no. 50, Jan. 2023, pp. 1–6.
[10] F. T. Li, Q. L. Xue, and J. Wang, "Influence of drilling fluid solid phase on performance of downhole turbo generator," *Mech. Sci. Technol.*, vol. 40, no. 2, pp. 193–197, Apr. 2021.
[11] Y. Xiao, Z. Zhang, M. S. Duraij, T.-G. Zsurzsan, and M. A. E. Andersen, "Review of high-temperature power electronics converters," *IEEE Trans. Power Electron.*, vol. 37, no. 12, pp. 14831–14849, Dec. 2022.
[12] X. Zhang, J. L. Han, and X. M. Zhang, "Progress in finite element analysis of accelerated reliability," *Equip. Environ. Eng.*, vol. 18, no. 9, pp. 27–34, Sep. 2021.
[13] J. Zhang, W. Lan, C. Deng, F. Wei, and X. Luo, "Thermal optimization of high-temperature downhole electronic devices," *IEEE Trans. Compon., Packag., Manuf. Technol.*, vol. 11, no. 11, pp. 1816–1823, Nov. 2021.
[14] S. Ma, S. Zhang, J. Wu, Y. Zhang, and W. Chu, "Experimental study on active thermal protection for electronic devices used in deep-downhole-environment exploration," *Energies*, vol. 16, no. 3, pp. 1231–1247, Dec. 2023.
[15] S. Dey, A. Mallik, and N. Goldsman, "High temperature application of a SiC-LDMOSFET based DC–DC power converter," in *Proc. WiPDA*, vol. 11, no. 59, Nov. 2021, pp. 333–338.
[16] L. Zhang, P. Liu, and S. Guo, "Comparative study of temperature sensitive electrical parameters for junction temperature monitoring in SiC MOSFET and Si IGBT," in *Proc. WiPDA*, vol. 11, no. 59, Nov. 2016, pp. 905–909.
[17] R. Beckwith, "Downhole electronic components: Achieving performance reliability," *J. Petroleum Technol.*, vol. 65, no. 8, pp. 42–57, Aug. 2013.
[18] C. Ma, Y. Tu, Y. Ren, S. Zhou, and Z. Z. Wang, "Review of thermal characteristics simulation analysis of electronic components," in *Proc. ICEPT*, vol. 40, no. 12, Aug. 2022, pp. 1–5.
[19] S. Dey, A. Mallik, N. Goldsman, and Z. Dilli, "Temperature dependent characterization based design optimization of a DC–DC converter for high-temperature applications," in *Proc. APEC*, vol. 24, no. 12, Mar. 2022, pp. 2034–2039.
[20] A. R. M. Siddique, H. Muresan, S. H. Majid, and S. Mahmud, "An adjustable closed-loop liquid-based thermoelectric electronic cooling system for variable load thermal management," *Thermal Sci. Eng. Prog.*, vol. 10, pp. 245–252, May 2019.
[21] J. Xiao, "Design of an active clamp flyback AC-DC converter control chip," M.S. dissertation, School Microelectron., Xidian Univ., Xi'an, China, 2022.
[22] L. Yimin, "Research and design of multiplex output power supply based on flyback converter," M.S. dissertation, School Automat., Nanjing Univ. Inf. Sci. Technol., 2022.
[23] D. Đ. Vracar, "Quasi-resonant flyback converter as auxiliary power-supply of an 800 V inductive-charging system for electric vehicles," *IEEE Access*, vol. 10, pp. 109609–109625, 2022.
[24] Y.-T. Yau and T.-L. Hung, "A flyback converter with novel active dissipative snubber," *IEEE Access*, vol. 10, pp. 108145–108158, 2022.
[25] J. Watson and G. Castro, "A review of high-temperature electronics technology and applications," *J. Mater. Sci.*, vol. 26, no. 12, pp. 9226–9235, Jul. 2015.
[26] S. Verma and Q. Elias, "Thermal management of electronics used in downhole tools," in *Proc. ATCE*, vol. 4, no. 88, Oct. 2012, pp. 8–10.
[27] M. Wei, W. Cai, M. Xu, and S. Deng, "Active cooling system for downhole electronics in high-temperature environments," *J. Thermal Sci. Eng. Appl.*, vol. 14, no. 8, pp. 8–16, Jan. 2022.
[28] Y. G. Lv, W. X. Chu, and Q. W. Wang, "Thermal management systems for electronics using in deep downhole environment: A review," *Int. Commun. Heat Mass Transf.*, vol. 139, no. 10, pp. 34–42, Dec. 2022.
[29] H. Zhang, W. Wang, and J. J. Deng, "Optimal design of heat dissipation on low power PCB," *Ferroelectrics*, vol. 595, pp. 59–147, Aug. 2022.
[30] Z. Ru, J. Q. Wu, M. Y. Li, X. F. Wang, and J. H. Tu, "Technology specification for derating of electronic components of switching power supply," in *Proc. CPSS*, Sep. 2021, pp. 2–5.
[31] L Chao L, X. J. Huang, Y. X. Xiao, W. H. Ma, and S. B. Jia, "Discussion on high temperature circuit design method of downhole instrument," *Chem. Enterprise Manag.*, vol. 373, no. 14, pp. 121–123, May 2015.
[32] *Test Methods and Procedures for Microelectronic Devices*, document GJB 548B-2005, 2005.

FEI LI received the bachelor's and master's degrees from Xi'an Jiaotong University, in 2000 and 2003, respectively, and the Ph.D. degree in electronics and electrical engineering from the University of Strathclyde, in 2006. In 2018, he returned to work with Xi'an Shiyou University. His research interest includes the research and development of key technologies in rotary-steerable drilling.

YUAN LIU received the bachelor's degree from Xi'an Shiyou University, in 2021, where he is currently pursuing the master's degree. His research interests include high-temperature power electronic technology and the research and design of DC–DC power supplies.

XUEYING MA received the bachelor's and master's degrees from Xi'an Shiyou University, in 2020 and 2023, respectively. Her research interests include power drive systems, hardware-in-the-loop simulation of virtual electric machines, and the study of motor control theories.

YUQI TAN received the master's degree from Xi'an Shiyou University, in 2022. His current research interest includes the study of high-reliability direct current power supplies.